# Adsorption Behavior of Organic Corrosion Inhibitors on Metal Surfaces—Some New Insights from Molecular Simulations

*Sumit Sharma,* Xueying Ko,* Yathish Kurapati,* Himanshu Singh,* and Srdjan Nešić‡,**

*Some recent efforts toward studying adsorption, aggregation, and self-assembly of corrosion inhibitor molecules near metal/water interfaces via classical molecular simulations are reported. Two different approaches have been used. In the first approach, a coarse-grained model of corrosion inhibitor molecules is studied, and the following key findings are found: (a) hydrophobic interactions between the alkyl tails of corrosion inhibitor molecules are important for the formation of adsorbed self-assembled layers on the metal surface, (b) the morphology of the adsorbed layers are strongly influenced by molecular geometry, and (c) the relative strength of interactions between polar head and metal and between alkyl tail and metal are important determinants of adsorbed conformations. In the second approach, fully atomistic simulations are performed for a bulk aqueous phase and near metal/water interfaces of two kinds of model inhibitor molecules—imidazolinium-type and quaternary ammonium-type surfactants. From these simulations, the following are concluded: (a) these inhibitor molecules aggregate in the bulk phase as spherical micelles, (b) the unaggregated inhibitor molecules have a strong tendency to adsorb onto metal surfaces while inhibitor micelles show only a weak tendency to adsorb, and experience a long-range repulsion from the surface. Finally, it is discussed how the coarse-grained and fully atomistic simulations present a unified molecular picture of adsorption and self-assembly of corrosion inhibitor molecules on metal surface.*

KEY WORDS: adsorption, corrosion inhibitor, micellization, molecular simulation, self-assembly

## INTRODUCTION

Corrosion inhibitors are generally defined as chemical substances that are added to the corrosive environment in very small quantities (typically in the ppm range) in order to mitigate corrosion. When it comes to internal corrosion of pipelines in the oil and gas industry, corrosion inhibitors are usually injected into the flow stream as a mixture of chemicals containing surfactant molecules.[1] The so-called "active component" in this mixture is most commonly an organic surfactant compound(s) with an amphiphilic molecular structure, consisting of a polar head group and nonpolar hydrophobic tail. The polar head is often based on nitrogen-containing groups, such as amines, amides, quaternary ammonium, or imidazoline-based salts as well as other functional groups containing oxygen, phosphorus, and/or sulfur atoms. The length of a hydrocarbon tail which is attached to a polar group typically varies between 12 and 18 carbon atoms. The function of the polar head-groups is to provide a bonding between inhibitor molecules and the steel surface. Hydrophobic tails which are "facing" the solution are thought to be important in establishment of self-assembled layer(s) of corrosion inhibitors on the metal surface[2] and key to the protection they offer.

While corrosion inhibitors have been used in the oil and gas industry for many decades, the mechanisms by which these molecules are effective in retarding corrosion are still poorly understood. As a result, unforeseen corrosion-related failures of inhibited oil and gas pipelines remain a major concern for the industry.

One can imagine that the effectiveness of corrosion inhibition depends on the adsorption characteristics of these molecules. Over the years, there were many experimental studies of adsorption behavior of corrosion inhibitors, deploying advanced techniques such as electrochemical impedance spectroscopy (EIS),[3-5] atomic force microscopy (AFM),[6-7] laser scattering,[8] quartz crystal microbalance (QCM),[7,9] sum frequency generation microscopy (SFG),[10] etc. It has generally been established that corrosion inhibitor molecules adsorb onto metal surfaces in organized self-assembled layers.

In parallel with the experimental studies, some computational investigations have been undertaken. There are quantum-mechanical studies based on density functional theory (DFT), wherein the focus is to determine binding energies of different polar groups on metal surfaces.[11-13] DFT calculations determine the equilibrium electronic structure, and no information on atomic motion at finite temperatures is obtained. For this purpose, classical molecular dynamics (MD) simulations are useful, wherein atomic motion can be simulated at finite temperatures. Classical MD simulations, so far, have mainly focused on studying equilibrium conformations of a single corrosion inhibitor molecule adsorbed onto metal surfaces.[14-15]

The results from experimental studies of inhibitor adsorption inevitably produce information that is spatially and

Submitted for publication: July 17, 2018. Revised and accepted: October 2, 2018.
Preprint available online: October 2, 2018, https://doi.org/10.5006/2976.
‡ Corresponding author. E-mail: nesic@ohio.edu.
* Institute for Corrosion and Multiphase Technology, Ohio University, Athens OH 45701.


ISSN 0010-9312 (print), 1938-159X (online) 

temporally averaged, with maximum resolution of the order of nanometer and microsecond, respectively. These length- and time-scales are much larger than those associated with behavior of individual inhibitor molecules and are more pertinent to behavior of large groups of molecules, adsorbed on the metal surface in the form of self-assembled layers. From experimental results, molecular-level behavior is indirectly deduced. In order to connect molecular behavior to experimental observations, the focus was shifted in this study from simulations of adsorption of individual molecules to classical MD simulations of a large number of molecules to examine their aggregation, adsorption, and self-assembly at the metal surface. The underlying free energy landscape of these systems was analyzed using advanced simulation methodologies and is described below. Unique insights obtained from classical MD simulations, which cannot be obtained either by experimental investigations or by DFT simulations, are highlighted.

## MOLECULAR DYNAMICS SIMULATIONS RESULTS AND DISCUSSION

The work described below is probing molecular-level details of adsorption of corrosion inhibitors on metal surfaces by using classical MD simulations. Before embarking on the discussion of the results, a brief overview of basic MD simulation concepts and terminology will be useful.

The dictionary meaning of simulation is "an imitative representation of the functioning of a system or process." As the name suggests, in MD simulations, dynamics/motion of molecules in the system is simulated. The term "classical" implies that in MD simulations, atomic and molecular motions are described by classical Newtonian mechanics (and not by quantum mechanics).[16] Often the term "classical" is dropped from the name. MD simulations can be performed at different resolutions. If each atom in the system is explicitly represented then these are termed as atomistic MD simulations. If many atoms are grouped together into a representative united atom or a "bead," then a molecule may be represented by a collection of beads or just one bead. Such simulations are termed coarse-grained (CG) MD simulations.

The term "molecular simulations" is used to collectively refer to all kinds of MD (as well as Monte Carlo) simulations. In an atomistic MD simulation, the simulated system is specified as a collection of atoms in a volume. Atoms interact with each other through a variety of conservative forces, such as: van der Waals, Coulomb, bond forces, etc. Each type of conservative force is associated with their potential energy. Fundamentally, all of these forces are electrostatic in nature, but they have different magnitudes and distance-dependence. Hence, the distance-dependence of potential energies of these forces are described by mathematical functions. These mathematical functions are termed *potential* for short and are collectively called a *force field*. Hence, for any configuration of atoms, the force acting on every atom can be calculated from the force field. In a CG system, the force field represents distance-dependence of potential energies between different beads in the system, rather than between each atom.

In a MD simulation, starting from an initial configuration of a number of atoms/beads in a given volume, the position and velocity of each atom/bead is determined at different times by performing a time-integration of Newtonian equations of motion. As the magnitude of forces between atoms/beads is distance-dependent, the simulated system is evolved by calculating forces between atoms/beads after every small time-step.

The required order of magnitude of the time-step in atomistic MD simulations is $10^{-15}$ s (femtosecond).[16] Hence, an atomistic MD simulation spanning 1 ns will require about a million evaluations of forces for every atom in the system. Because of the computational complexities involved, atomistic MD simulations are generally only able to sample time-scales of the order of 1 ns to 1,000 ns. In the case of CG MD simulations, the accessible time-scales may be one to three orders of magnitude larger because of the reduced number of degrees of freedom.

From the positions and trajectories of atoms/beads thus obtained, thermodynamic properties of the simulated system are evaluated by applying the basic concepts of statistical mechanics. Statistical mechanics is a branch of physics that describes the relationship between molecular-level properties and macroscopic thermodynamic properties. The basic tenet of statistical mechanics is that statistical properties of molecular configurations correspond to thermodynamic properties. For example, average translational kinetic energy is related to thermodynamic temperature, average total energy of molecules corresponds to thermodynamic energy, total number of possible molecular configurations is related to thermodynamic entropy, etc.

Molecular simulations have emerged as a powerful tool to study physical properties of systems. The focus here was on applying MD simulation techniques to understand the adsorption and aggregation behavior of corrosion inhibitor molecules on the metal surface. In the text below, the simulation strategies and major findings are described.

### *2.1 | Coarse-Grained Molecular Dynamics Simulations of Corrosion Inhibitor Adsorption*

Generally, collective behavior of large swarms of molecules require long time- and length-scales, for example, in phase transition, during self-assembly and formation of equilibrium morphologies of adsorbed molecules, etc. CG molecular simulations are useful for studying these phenomena, as specific chemical details of molecules are not resolved. Rather, potential functions are used to represent overall effective interactions between different segments of the molecules, making the simulated system simpler, and the numerical simulations faster. Hence, one can perform simulations that can cover the required time- and length-scales, in this case those related to forming equilibrium morphologies by corrosion inhibitors adsorbing on a metal surface.

In terms of previous studies using a similar CG approach, Duda, et al., performed a Monte Carlo study of adsorption of CG corrosion inhibitor molecules in two dimensions to show that the surface coverage improves with tail-length, $m_T$ up to $m_T = 7$ and with solvophobicity of corrosion inhibitor molecules.[17] Wu, et al., studied micellization of CG ammonium-based surfactants, and found that the surfactants form spherical micelles at smaller aggregation numbers (<100) and worm-like micelles at larger aggregation number.[18] Edwards, et al., created a hexagonal close packing of different imidazoline-based inhibitor molecules, represented by a CG model, on a surface and performed MD simulations to determine available free volume for diffusion of corrosive species.[8] These studies have aided in the understanding of how corrosion inhibitor molecules aggregate and adsorb on surfaces to inhibit corrosion. A caveat of CG is that some degrees of freedom are lost (such as the rotational motion of an alkyl tail around dihedral angles) and, therefore, there is some loss of entropic terms. Therefore, an effective CG methodology should be such that the important degrees of freedom are retained while relatively less relevant ones are restricted.

Apart from verifying theoretical hypotheses, MD simulations can be used as a predictive tool for inhibitor performance. In the present study, systematic investigations of how lateral hydrophobic interactions, the interactions between metal surface and inhibitor molecules, and inhibitor geometry affect the adsorption, self-assembly, and aggregation behavior of these molecules are performed by studying a phenomenological bead-spring model of these molecules.[19]

### 2.1.1 | Simulation Setup and System Details

In the CG approach, the corrosion inhibitor molecule is understood to be comprised of two basic parts: a polar group that has a strong affinity to bind to the metal surface, and a hydrophobic group that has the ability to form some kind of a "hydrophobic barrier" when organized in self-assembled layer at the metal/water interface. The basic approach behind the design of the present CG model of corrosion inhibitor molecules is to incorporate these two features into the model and examine the adsorption and self-assembly behavior.

#### 2.1.1.1 | Potential Functions in the Coarse Grained Model

In the CG description of an amphiphilic corrosion inhibitor molecule, one terminal bead represents the polar head group of the molecule and the remaining beads represent the hydrophobic alkyl tail segments (Figure 1[a]).[19] A number of such corrosion inhibitor molecules are randomly placed in a simulation volume (also called a simulation box), as shown in Figure 1(b). This configuration serves as an initial condition for the MD simulations.

Bond interactions between neighboring beads in an inhibitor molecule keep them together and are modeled via a quadratic function, also termed harmonic bond potential, given by:

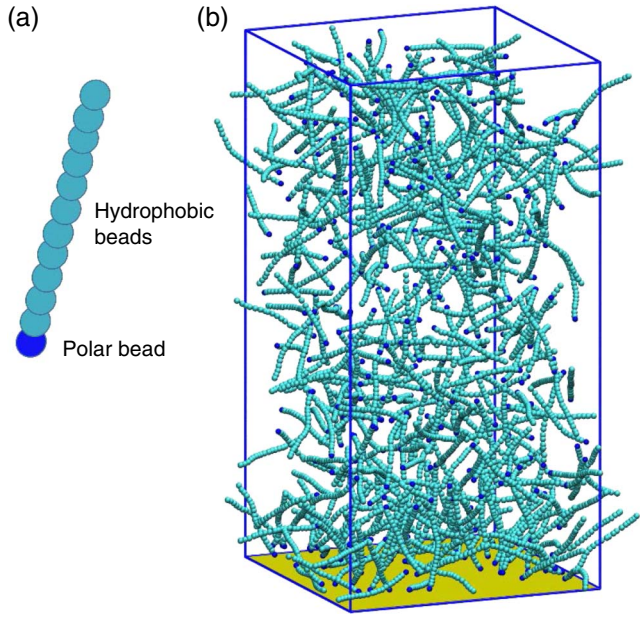


**FIGURE 1.** *(a) A schematic of the CG corrosion inhibitor molecule used in the present study. The blue terminal bead represents the polar head group and the cyan beads represent the alkyl tail segments. (b) A snapshot of simulation system with the simulation volume and the randomly distributed corrosion inhibitor molecules. The yellow plane at the bottom represents the metal surface.*

$$U_b = k_b(b - b_0)^2 \quad (1)$$

where $k_b$ is the bond coefficient which determines the stiffness of the bond potential, b is any instantaneous value of the bond length, and $b_0$ is the equilibrium value of the bond length between the neighboring beads. Along with the bond potential, a harmonic angle potential centered at $\theta_0$ is also applied. The functional form of this potential is given by:

$$U_\theta = k_\theta(\theta - \theta_0)^2 \quad (2)$$

where $k_\theta$ is the angle coefficient of the potential, θ is the instantaneous value of the angle, and $\theta_0$ is the equilibrium value of the angle between any three neighboring beads. The angle potential ensures that the angle between three neighboring beads in a molecule is maintained close to $\theta_0$ (often equal to 180° for a linear geometry).

Water molecules are not explicitly included in the CG simulation system, but their effect on the interactions between inhibitor molecules and on the dynamics of inhibitor molecule motion is implicitly included, as described below.

In an aqueous environment, hydrophobic beads manifest an attractive interaction amongst themselves. In the model, this attractive interaction between hydrophobic tail beads of different inhibitor molecules is represented by a Lennard-Jones (LJ) interaction potential, given by:

$$U_{LJ}(r) = 4\varepsilon\left(\left(\frac{\sigma}{r}\right)^{12} - \left(\frac{\sigma}{r}\right)^{6}\right) \quad (3)$$

where ε is termed as the LJ potential well-depth. It signifies how "deep" the minimum of the LJ potential is (Figure 2); a large value of ε implies a more attractive LJ potential; σ is a measure of size of the beads, and r is the distance between the beads. The force between the beads is given by negative gradient of the potential energy, that is, $\vec{F} = -\nabla U$. This implies that for a LJ potential,

$$\vec{F} = 24\varepsilon\left(2\left(\frac{\sigma}{r}\right)^{12} - \left(\frac{\sigma}{r}\right)^{6}\right)\frac{\vec{r}}{r^2} \quad (4)$$

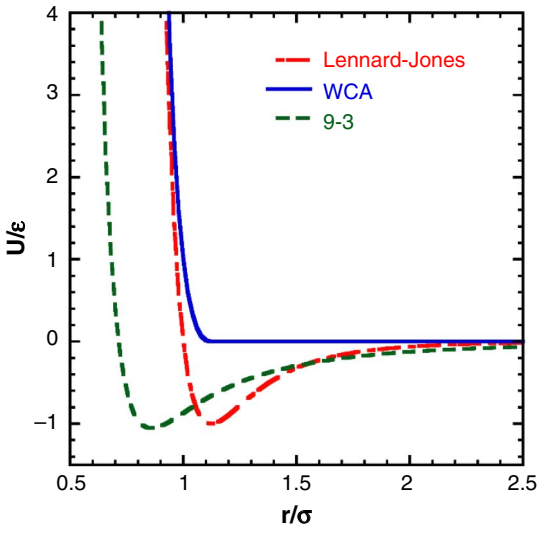


**FIGURE 2.** *Three different potential functions used in the CG model: LJ, WCA, and 9-3 potential plotted (scaled by ε) as a function of distance (scaled by σ).*

$\vec{F} = 0$ when $r = 2^{1/6}\sigma$. The LJ potential is attractive at large distances ($r > 2^{1/6}\sigma$) as for these values of r, $\vec{F}$ is in opposite direction as $\vec{r}$. The LJ potential is repulsive at small distances ($r < 2^{1/6}\sigma$) when $\vec{F}$ is in the same direction as $\vec{r}$. The form of the LJ potential function is plotted in Figure 2, where the potential energy is scaled by ε and the distance is scaled by σ.

The interaction between the polar head beads of different inhibitor molecules, as well as between the polar bead of one molecule and the hydrophobic beads of another, is represented by a purely repulsive Weeks-Chandler-Andersen (WCA) potential.[20] The WCA potential is simply modeled as the repulsive part of the LJ potential, given by:

$$U_{WCA}(r) = U_{LJ}(r) + \varepsilon \qquad \text{for } r < 2^{1/6}\sigma \tag{5}$$

and

$$U_{WCA}(r) = 0 \qquad \text{for } r > 2^{1/6}\sigma$$

This function is also shown in (Figure 2). The rationale behind using a purely repulsive WCA potential for polar beads is that in an aqueous environment, polar moieties have similar interactions with water molecules as with other polar and hydrophobic moieties. As a result, no net attractive interaction between different polar groups or between polar and hydrophobic groups is observed. The strong short-ranged repulsion of LJ and WCA potential represents the "excluded volume" interactions between the different groups.

The metal surface in the model is represented by a smooth, two-dimensional surface occupying one face of the simulation box. The strong affinity between the polar beads of the corrosion inhibitor molecules and the surface are modeled by a so-called "9-3" interaction potential given by:

$$U_{9-3}(z) = \varepsilon_s\left(\frac{2}{15}\left(\frac{\sigma}{z}\right)^9 - \left(\frac{\sigma}{z}\right)^3\right) \tag{6}$$

where $\varepsilon_s$ is the well-depth parameter, and z is the distance between the surface and the bead. Consider a slab of LJ atoms extending from z = 0 to $z \to -\infty$ and infinite in extent in the x and y directions. If a LJ atom is placed at a distance z > 0 from such a surface, then the net interaction potential is evaluated by integrating the contributions of all of the LJ atoms that comprise the surface. Such an integration leads to the 9-3 potential function with the factor $\varepsilon_s = \frac{2\pi\varepsilon_{surf}\rho\sigma_{surf}^3}{3}$ where $\varepsilon_{surf}$ and $\sigma_{surf}$ are LJ interaction parameters of surface atoms and ρ is the number density of atoms in the slab. For a hexagonal closed packing of LJ atoms with $\sigma_{surf} = 1$, the factor $\frac{2\pi\rho}{3} = 2.96$. The 9-3 potential is also plotted in Figure 2, scaled with $\varepsilon_s$. As a result of interaction contribution from a semi-infinite slab, the excluded volume of the 9-3 potential is smaller and the repulsive part is "softer" in comparison to the LJ potential. The 9-3 potential decays as $r^{-3}$, and therefore slower than the LJ potential with distance. The relative magnitudes of potential well-depth parameters, ε and $\varepsilon_s$, can be used to set the strengths of different bead interactions. In the first set of simulations, the interactions between hydrophobic beads of inhibitor molecules and the surface are set to zero. The underlying reason for this simplification is to study a minimalist model of inhibitor molecules wherein the effect of only two interactions is examined: (1) a strong interaction between the polar beads and the surface, and (2) hydrophobic interactions between the tails. In the subsequent set of simulations, the interactions between hydrophobic beads and metal surface are also modeled using the 9-3 potential function.

### 2.1.1.2 | Reduced Units and Simulation Parameters

In this sub-section, the concept of reduced units, which are commonly used in MD simulations, especially in CG systems, is briefly discussed. In reduced units, the units of energy, mass, and distance are defined in a manner so as to ease the computational expense in simulations.[16] For this system, the unit of energy is taken as thermal energy, $k_BT$, which is set equal to one, where $k_B$ is Boltzmann constant and T is the temperature. The potential well-depth, ε, has units of energy, and therefore is specified in terms of units of thermal energy. For example, ε = 0.5 implies that the potential well-depth is 50% of thermal energy. One can always convert from reduced units to real units and vice-versa. At 300 K, thermal energy is ~2.5 KJ/mol, so ε = 0.5 implies energy of 1.25 KJ/mol. Mass of each bead is set equal to one in reduced units, which can be understood as the mass of one alkyl monomer. The size of a bead, σ, is set to one in reduced units, which is equal to ~3 Å (0.3 nm). Hence, a length of, say 20 in reduced units is 60 Å (6 nm) in real units. Time in reduced units is calculated as $t = \sigma\left(\frac{m}{k_BT}\right)^{1/2}$. Hence, time of one in reduced units corresponds to ~7 ps in real units.

Now that appropriate reduced units have been defined, all system parameters can be specified in terms of these units. The LJ potential well-depth parameter for interactions between hydrophobic tails, ε is varied from 0.01 to 0.08 in the present simulations. For a corrosion inhibitor molecule of 20 beads (1 polar and 19 hydrophobic beads), the ε = 0.05 corresponds to ~1 $k_BT$ or 2.5 KJ/mol of interaction energy, which is of the same order of magnitude as the measured hydrophobic interaction between species of O (1 nm) in size.[21] The 9-3 potential well-depth parameter for interactions between a polar bead and the metal surface is $\varepsilon_s = 5$. This value corresponds to a binding energy of 12.5 KJ/mol, which is similar in magnitude to the values determined by the DFT calculations of polar groups on metal surface.[13]

The simulation box size is taken as 20 × 20 × 40 in the X, Y, and Z axes. The metal surface is at Z = 0, i.e., in the XY plane. On the opposite face of the simulation box, there is a noninteracting surface, or a reflection boundary, used to keep the number of inhibitor molecules fixed in the simulation system. The simulation system is periodic in the X and Y directions. A corrosion inhibitor molecule is comprised of 20 beads and there are 400 molecules in the simulation box. The equilibrium bond length is $b_0 = 0.3$, and equilibrium angle between beads in a molecule is $\theta_0 = 180°$. The value of the bond coefficient, $k_b$, is set to 100 $k_BT/\sigma^2$. The value of the angle coefficient, $k_\theta$, is set to 50 $k_BT/rad^2$. Therefore, the $k_b$ and $k_\theta$ are sufficiently stiff such that only small fluctuations in the bonds and the angles between the bonds of the corrosion inhibitor molecule are possible.

As the effect of solvent (water) in this simulation system is implicitly included, that is without having the actual water molecules accounted for, a Langevin dynamics simulation is performed to incorporate the effect of solvent on the dynamics of inhibitor molecules. In a Langevin dynamics simulation, each molecule in the system experiences a random Gaussian force as well as a viscous drag force.[16] These two forces replicate the numerous interactions between corrosion inhibitor molecules and water molecules that lead to Brownian motion of the inhibitor molecules.

Hence, the phenomenological CG model described above incorporates effective interactions between inhibitor molecules themselves in an aqueous environment and the inhibitor molecules and the metal surface. All simulations are performed using Large-Scale Atomic/Molecular Massively Parallel

Simulator (LAMMPS†) MD simulations package.[22] For each data point (discussed below), the simulations are performed in parallel on eight processors. Equilibrium is obtained after $2 \times 10^8$ to $6 \times 10^8$ MD time-steps, which took 3 weeks to 9 weeks to execute. The error bars in the data are generated from three to four different equilibrated simulation runs.

### 2.1.2 | Results

Simulations done using this CG model have provided interesting new insights into adsorption behavior of corrosion inhibitors on a metal surface. Some of the highlights are discussed below.

#### 2.1.2.1 | Hydrophobic Interactions of Inhibitor Tails Are Important in Adsorption

It is often presumed in the corrosion community that the main driver of adsorption of corrosion inhibitor molecules is the strong affinity between the polar head group and the metal surface. Therefore, many previous studies have focused on calculating binding energies of different polar groups on metal surfaces as a surrogate of adsorption efficiency.[12-13] However, some experimental evidence suggests that lateral hydrophobic interactions between the alkyl tails of surfactant molecules play an important role in the adsorption process.[23-26]

In order to elucidate the role of hydrophobic interactions in adsorption, a series of simulations was performed here, wherein the affinity between the hydrophobic tails of corrosion inhibitor molecules toward each other was varied by changing the well-depth of LJ interactions, ε. A small value of ε corresponds to weak affinity between the tails of corrosion inhibitor molecules, while a large value corresponds to strong affinity. In this set of simulations, the interaction strength between the polar head group of the inhibitors and the metal surface was kept constant ($\varepsilon_s = 5$).

Figure 3 shows equilibrium number of adsorbed corrosion inhibitor molecules, N, on the surface as a function of ε. It is seen that for small values of ε, i.e., when the affinity of hydrophobic tails towards each other is low, the adsorbed number of molecules on the metal surface is small, corresponding to low, random adsorption. As ε is increased, a dramatic rise in the N is observed. At the highest adsorbed amount (corresponding to $\varepsilon \approx 0.065$), a self-assembled monolayer (SAM) of adsorbed molecules is formed. When that optimum ε is exceeded, there is decrease in the number of adsorbed molecules as they tend to aggregate more strongly in the solution and make some sort of micelles. This is clearly illustrated in Figure 3, where the snapshots of the simulation box for three different values of ε show different adsorbed states.

To better understand the spatial distribution of adsorbed inhibitor molecules in the SAM formed on the metal surface, radial distribution function in the XY plane, RDFxy(r) is calculated. The RDFxy(r) shows local arrangement of other corrosion inhibitor molecules around any given molecule, by determining the average number of other molecules at a distance r in the XY plane from the center of that molecule. This number is divided by the number of molecules one would expect if the adsorbed molecules were uniformly distributed around the given molecule. Hence, an RDFxy(r) = 1 indicates that molecules do not have any specific spatial arrangement. Figure 4(a) shows RDFxy(r) of adsorbed molecules for $\varepsilon = 0.065$ and $\varepsilon = 0.03$. For $\varepsilon = 0.065$, the RDFxy(r) shows regular peaks as r increases, indicating that

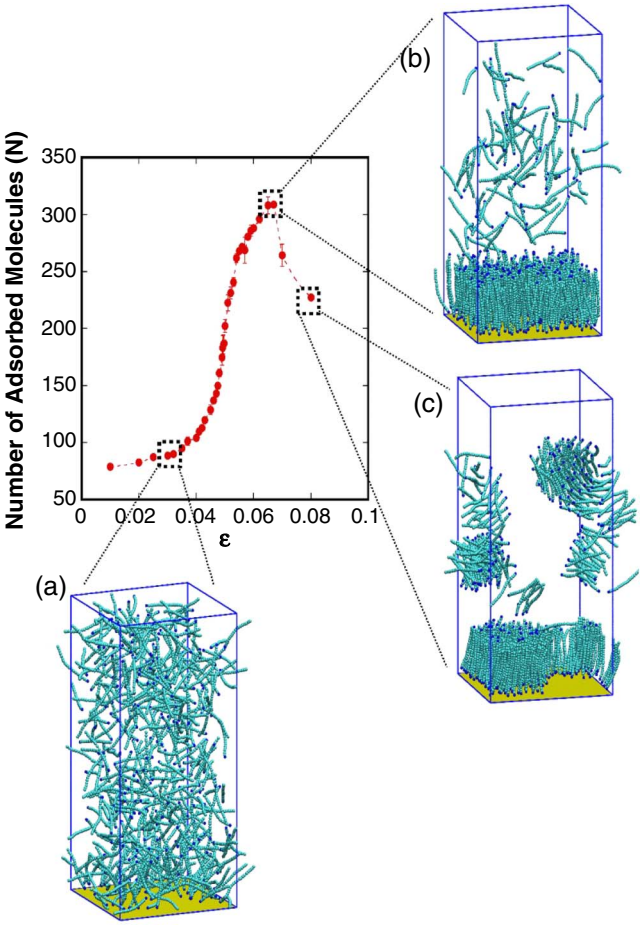


**FIGURE 3.** *The number of adsorbed molecules in equilibrium, N, as a function of the strength of hydrophobic interactions between inhibitor tails, ε. Snapshots of the simulation system at different ε values are also shown: (a) ε = 0.03: low, random adsorption; (b) ε = 0.065: adsorbed SAM; and (c) ε = 0.08: aggregated states in the bulk and the adsorbed phases.*

the adsorbed corrosion inhibitor molecules are arranged in a specific, well-defined arrangement. For $\varepsilon = 0.03$, RDFxy(r) ≈ 1 indicates random arrangement, i.e., low adsorption. Note that the RDFxy(r) is small for very small distances. This is simply a consequence of excluded volume of the molecules.

In order to further understand this adsorption behavior, the orientation factor of the adsorbed molecules and the molecules in the bulk phase have been calculated. The orientation factor, S, is defined as the largest eigenvalue of the tensor, Q, given by the following equation:[27]

$$Q_{\alpha\beta} = \frac{1.5}{N}\sum_{i=1}^{N} |n_{i\alpha} \times n_{i\beta}| - \frac{1}{2}\delta_{\alpha\beta} \qquad (7)$$

where $n_{i\alpha}$ and $n_{i\beta}$ are the α and β components of the end-to-end unit vector of molecule i, respectively. N is the total number of molecules, and $\delta_{\alpha\beta}$ is the Kronecker delta function defined equal to 1 when α = β and 0 otherwise. The value of S = 1 arises when all of the molecules are perfectly aligned parallel to each other, and S = 0.5 for a completely random orientation of molecules.

In the Figure 4(b), the S for molecules in the adsorbed layer and in the bulk phase (that is, in simulations with no surface

† Trade name.

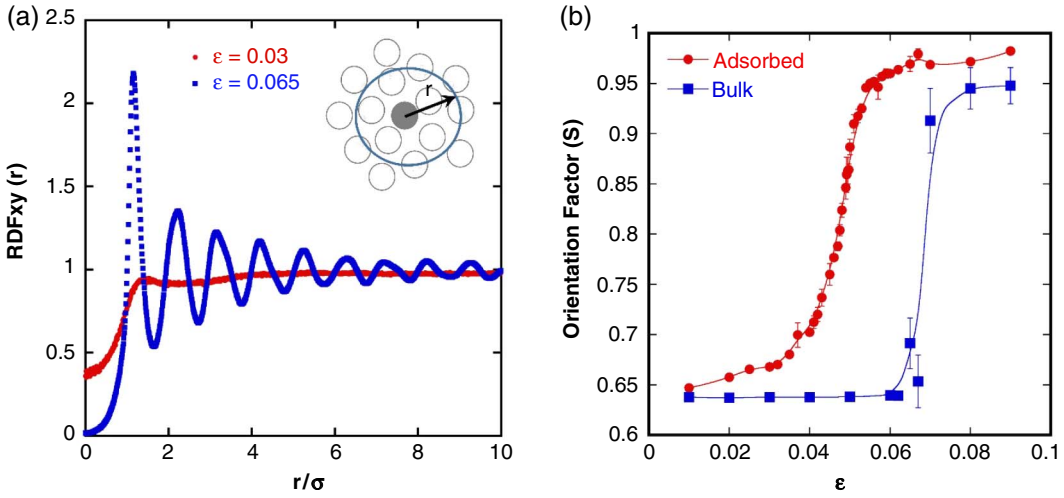


**FIGURE 4.** *(a) Radial distribution function in the XY plane, RDFxy(r) of adsorbed molecules for ε = 0.065 and ε = 0.03. The inset shows a schematic on how RDFxy(r) is calculated. (b) Orientation factor, S, of molecules in the adsorbed state and in the bulk phase as a function of ε. Adapted with permission from Ko and Sharma.*[19]

present) is plotted as a function of ε. For small values of ε (<0.04), S is small, which confirms that the molecules are adsorbed in random orientations. The value of S increases sharply with ε and S reaches close to 1 for the adsorbed phase for ε ≈ 0.065. This observation shows that for the values of ε ≈ 0.065, the tails of adsorbed molecules are aligned parallel to one another, forming a SAM. In the bulk phase, a significant increase in S is observed only for values of ε ≥ 0.07; however, at the same time a decrease in the adsorption is observed (Figure 3). For these large values of ε, the molecules start aggregating in the bulk phase as well. Hence, one can conclude that adsorption decreases when the molecules start aggregating in the bulk as micelles. These results show that by simply changing the strength of hydrophobic interactions between corrosion inhibitor tails, a significantly different adsorption behavior is observed.

### *2.1.3 | Adsorption Morphologies Depend on the Geometry of Corrosion Inhibitor Molecules*

An area that has received little attention in the corrosion literature is the morphology of adsorbed corrosion inhibitors on metal surfaces. With the rationale being that strong affinity between the polar head groups and the metal surface is a prerequisite for good adsorption, often surfactants with bulky head groups comprised of aromatic or heterocyclic rings are tested for corrosion inhibition.[1] By doing this, the effect of molecular geometry on the adsorption behavior is not taken into consideration properly. To determine the effect of molecular geometry, the effect of a large head group on the aggregation and adsorption behavior of inhibitor molecules was studied in this CG model system.

This was done by changing the size of the polar head bead to make it twice that of the hydrophobic beads, that is $\sigma_P = 2\sigma$. In this case it was found that the inhibitor molecules aggregate in the bulk as well as adsorb on the metal surface as cylindrical micelles (Figure 5).[19] The shape of micelles could be determined by calculating various shape factors, such as acylindricity and asphericity. These shape factors are calculated from the principle eigenvalues of the radius of gyration squared tensor of the micelles.[19,28] The acylindricity and asphericity of micelles of inhibitor molecules in the bulk and in the adsorbed layer are shown in Figure 5(a). A perfect sphere will have an asphericity value of 0. Similarly, a perfect cylinder will have the acylindricity value of 0.

Clearly, acylindricity is small in both phases, while asphericity is high, indicating that the micelles are cylindrical in shape. The molecules aggregate to form micellar structures that maximize interactions among themselves, or equivalently, minimize the exposed surface area. It can be imagined that a larger head group will lend asymmetry in the molecular geometry, because of which laminar packing of the molecules will be inefficient in maximizing their interactions. Based on geometrical arguments, optimum micellar shapes can be predicted by critical packing parameter (CPP).[29] CPP is a dimensionless number, given by V/(AL) where V is the volume of the tail, A is the area of the head group, and L is the tail length. Assuming the tail to be a cylinder of excluded volume, $V = \frac{\pi\sigma^2 L}{4}$ and $A = \frac{\pi}{4}\left(\frac{\sigma_P+\sigma}{2}\right)^2$, CPP ≈ 0.44, which corresponds to cylindrical micelles.[29]

These results corroborate previous AFM results, wherein it is observed that surfactants can adsorb onto surfaces in micellar structures similar to those observed in the bulk phase.[30-31] One would further assume that the morphology of the adsorbed layer will have an effect on the interfacial properties. Hence, these results suggest that molecular geometry particularly that of the head group is an important consideration that should be accounted for while designing effective corrosion inhibitor molecules. These initial CG simulations suggest that inhibitor molecules with bulky head groups probably lead to less effective SAM.

#### *2.1.3.1 | Kinetics of Adsorption Is Related to Different Stages of Self-Assembly of the Surface Layer*

The kinetics of adsorption and self-assembly of corrosion inhibitors to form surface layers were investigated next. It is to be noted that while the experimental kinetics studies often take hours or even days to reach a steady state, in molecular simulations much smaller time-scales are accessible. In the simulations one can overcome the diffusional barrier by studying adsorption at much higher concentrations of corrosion inhibitor molecules than those used in experiments. In this case, the kinetics obtained in the simulations may only be

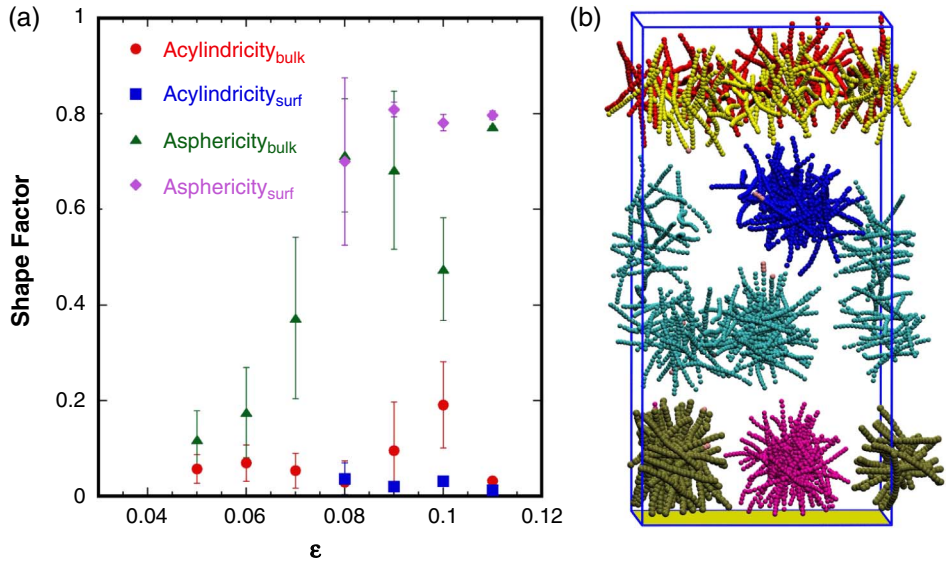


**FIGURE 5.** *(a) Acylindricity and asphericity shape factors of micelles of inhibitor molecules in the adsorbed and the bulk phase as a function of ε. (b) A snapshot of the simulation system for ε = 0.11. Different micelles are identified by different colors for ease of visualization. Adapted with permission from Ko and Sharma.*[19]

qualitatively compared to the experiments, yet the qualitative conclusions remain valid.

Figure 6(a) shows adsorption kinetics of corrosion inhibitor molecules ($\sigma_P = \sigma$, $\varepsilon = 0.065$, $\varepsilon_s = 5$). Along with the total number of molecules adsorbed, N, the number of adsorbed molecules with their polar group pointing towards the surface is also plotted. The observed kinetics may be approximately considered as occurring in three stages. In the first stage, the adsorption kinetics are fast and most molecules adsorb with their polar group toward the surface. Figure 6(b) shows average number of distinct clusters of adsorbed molecules as a function of N. In the first stage, roughly 1/3 of the equilibrium amount is adsorbed and the adsorbed molecules form distinct clusters on the surface. In the second stage, the rate of adsorption is slower and some molecules adsorb with their polar groups pointing away from the surface. In the second stage, close to 80% of the equilibrium amount is adsorbed. The number of distinct clusters decreases in this stage, indicating that the clusters grow in size and merge with each other. By the end of the second stage, all of the clusters merge together into one, forming an adsorbed layer of inhibitor molecules. In the final third stage of adsorption, no further increase in the adsorbed molecules with their polar group pointing toward the surface is observed. All of the molecules adsorb with their polar group away from the surface.

It is to be noted that many previous researchers have studied adsorption kinetics of surfactant molecules on different surfaces using a QCM. They have reported multistage adsorption kinetics and have hypothesized the adsorption mechanism qualitatively similar to what was observed in the present kinetics study.[32-34]

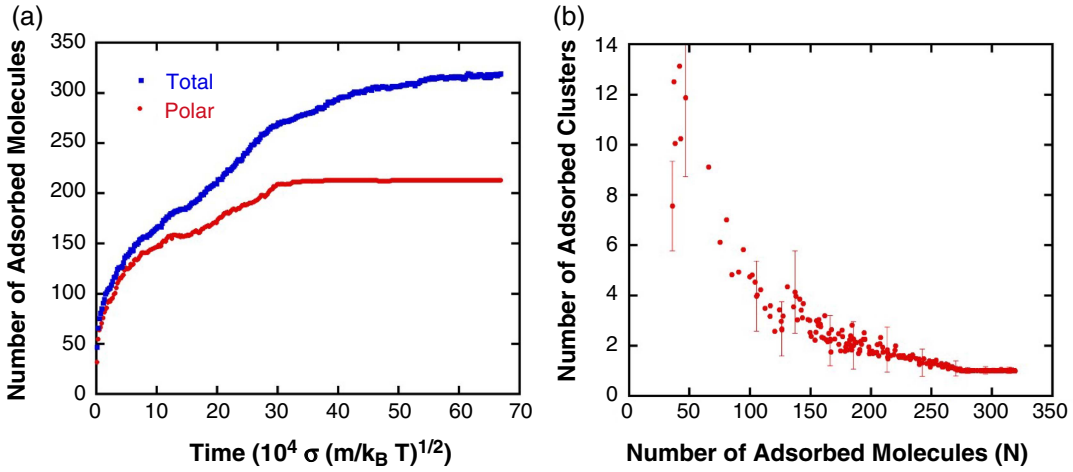


**FIGURE 6.** *Kinetics of adsorption of molecules. (a) The red line shows adsorption of molecules with their polar group toward the surface; the blue line shows total number of adsorbed molecules. (b) Number of distinct adsorbed clusters of molecules identified as a function of the number of adsorbed molecules, N.*

### 2.1.3.2 | Strong Interactions Between Inhibitor Tail and Metal Surface Alter Adsorbed Conformations

In the simulations discussed above, the interactions between alkyl tails and metal surface have been ignored. The rationale was to develop a minimalist model of inhibitor molecules wherein the effects of a strong polar group-metal interaction and hydrophobic interaction between tails are studied. In this section, the simulation results are discussed wherein the interactions between alkyl tails and metal atoms were incorporated in the model. With the inclusion of interactions between tail and surface, an inhibitor molecule will have a preference to adsorb in two different configurations: the first one being "lying-down" on the surface, and second one being "standing-up" with only the polar group interacting with the surface. In case of isotropic interactions between species, the "lying-down" configuration will be preferred in the dilute limit as this will allow the polar bead, as well as the tail, to interact with the surface. On the other hand, when the adsorbed concentration of inhibitor molecules increases, the molecules may prefer to attain the "standing-up" configuration as this will allow (a) more molecules to adsorb with their polar group interacting with the surface, and (b) hydrophobic interactions between the tails of standing-up adsorbed inhibitor molecules. The effect of tail-metal interactions on the adsorption behavior can be understood by a theoretical model illustrated below.

Consider a linear corrosion inhibitor molecule, which can thought of as a cylinder of cross-sectional area $A_c$, length l, and diameter d. Let $\varepsilon_s$ be the interaction between a polar group and the surface; $\varepsilon$ be the hydrophobic interaction between alkyl beads; and $\varepsilon_t$ be the interaction between an alkyl bead and the surface. The total energy of interaction in the lying-down configuration of a molecule is given by:

$$E_{lying} = \varepsilon_s + n\varepsilon_t \quad (8)$$

where n is the number of beads in the alkyl tail. As the adsorption concentration increases, the molecules will prefer to stand-up if the adsorption of more molecules in the standing-up configuration is energetically favorable. The relative magnitude of the energy associated with the standing-up and lying-down configurations can be compared by the following ratio:

$$\frac{E_{standing}}{E_{lying}} = \frac{l\,d\,f}{A_c}\frac{\varepsilon_s}{\varepsilon_s + n\varepsilon_t} \quad (9)$$

where f is the packing efficiency of molecules in the standing-up configuration. For this CG model of corrosion inhibitors: $l = 6\sigma$, $d = \sigma$, $f = 0.62$, $A_c = \pi d^2/4$, and $n = 19$. The value of f is calculated from the result that on an average 315 molecules adsorb in the SAM configuration on the $20\,\sigma \times 20\,\sigma$ surface (Figure 3). To test the validity of this theoretical model, molecular simulations of systems have been performed with different values of polar group-surface interaction, $\varepsilon_s$, and tail-surface interaction, $\varepsilon_t$, with tail-tail interaction $\varepsilon$ fixed at 0.065. $\varepsilon = 0.065$ is chosen because a SAM is formed for this value (Figure 3).

Figure 7 summarizes the simulation results. The blue square points represent simulations in which a standing-up configuration (eventually leading to the formation of SAM) of molecules in the adsorbed state is formed. The red circle points represent simulations in which lying-down configuration of molecules is observed. The line represents the theoretical model when the ratio $\frac{E_{standing}}{E_{lying}} = 1$ (Equation [9]). The theoretical model seems to be quantitatively accurate in delineating the lying-down and standing-up configurations. The one mismatch at $\varepsilon_s = 3$ and $\varepsilon_t = 0.5525$ is probably because, for these strong tail-surface interactions, the energy penalty for a molecule to stand-up is large. As a result, the molecules are kinetically trapped in the lying-down configurations. From Figure 7 and this theoretical model, it is clear that a strong interaction between the polar head and the surface is favorable for the formation of a well-packed SAM of adsorbed molecules.

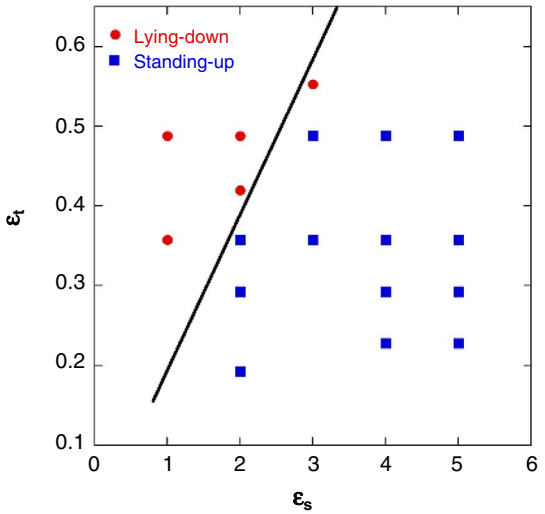


**FIGURE 7.** *Summary of simulation results performed with different values of $\varepsilon_s$ and $\varepsilon_t$. The black line indicates the theoretical condition of $E_{standing} = E_{lying}$ as per Equation (9). It is observed that the theoretical prediction is quite accurate in predicting adsorbed conformations of the molecules.*

In the case of standing-up configuration, eventually a SAM of adsorbed molecules is formed. In the case of lying-down configuration, multiple layers of adsorption are seen with molecules stacking on top of each other. Figure 8 shows distribution profiles of equilibrium-adsorbed configurations obtained for (a) the standing-up case ($\varepsilon_s = 2$ and $\varepsilon_t = 0.3575$), and (b) the lying-down case ($\varepsilon_s = 2$ and $\varepsilon_t = 0.4875$) as a function of distance from the surface, z. A single peak in case (a) shows formation of a SAM, while multiple, periodic peaks in case (b) show stacking up of molecules. The distribution profile is obtained by counting the average number of molecules at a distance z from the surface and dividing it by the average number one would expect in the case of uniform distribution of molecules in the entire simulation box.

In summary, through a simple CG representation of corrosion inhibitor molecules, some interesting insights into the adsorption and self-assembly behavior of these molecules are obtained. An important learning is that a strong affinity between the polar group and the metal surface is not sufficient for good adsorption. The lateral hydrophobic interactions between tails play an important role in adsorption. Another interesting result is that the morphology of the adsorbed surfactant film will likely depend on the molecular geometry. Furthermore, the kinetics of formation of adsorbed inhibitor film reveal that the initial adsorption is dominated by the interaction between polar group and the metal surface, but the subsequent adsorption is driven by lateral hydrophobic interactions. Lastly, strong interactions between alkyl tail and metal surface may alter the adsorbed conformations.

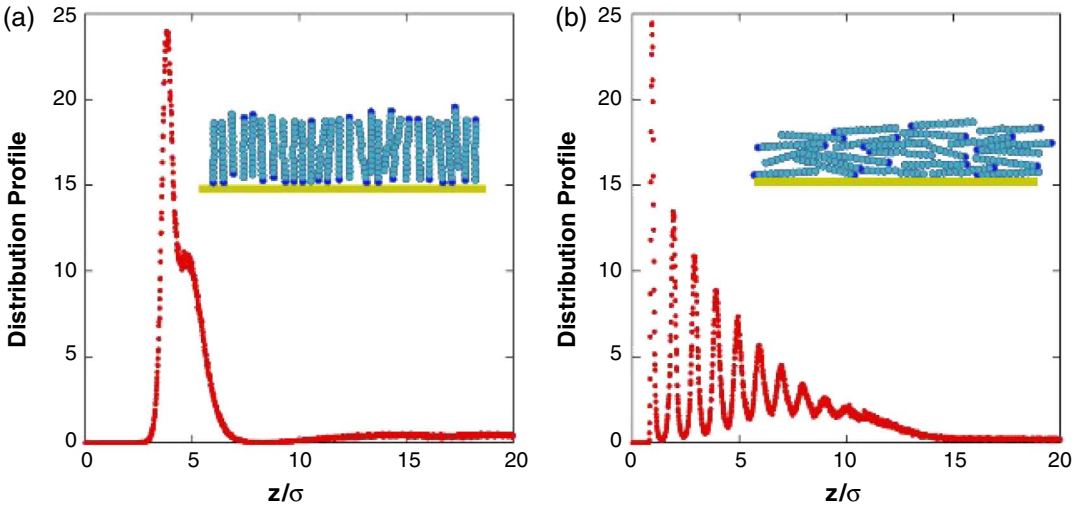


**FIGURE 8.** *Distribution profile of center of mass of corrosion inhibitor molecules in the equilibrium configurations as a function of distance from the surface, z, for (a) $\varepsilon_s = 2$ and $\varepsilon_t = 0.3575$, and (b) $\varepsilon_s = 2$ and $\varepsilon_t = 0.4875$. From Figure 7, it is seen that the case (a) corresponds to that of standing-up configurations, which leads to formation of a SAM. Therefore, the distribution profile shows a peak and a shoulder. The case (b) corresponds to the lying-down configurations. This eventually leads to multiple layers of adsorbed molecules in the lying-down configurations. Hence, the distribution profile shows periodic peaks. The insets show illustrations of the final adsorbed configurations in the two cases.*

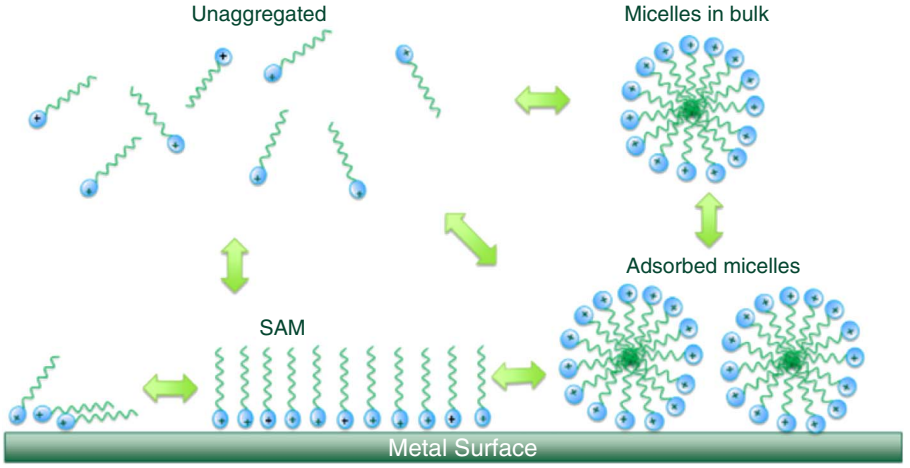


**FIGURE 9.** *A schematic showing some possible states of corrosion inhibitor molecules in bulk aqueous phase and near metal/water interfaces.*

### *2.2 | Atomistic Molecular Dynamics Simulations of Corrosion Inhibitors*

While CG models are suitable for studying longer time-scale and larger length-scale adsorption and self-assembly behavior of larger numbers of inhibitor molecules, atomistic simulations are more useful for studying smaller number of molecules over shorter time- and length-scales, while enabling one to use full chemical detail in the definition of the molecules. The goal here was to use atomistic modeling to determine relative stability of different states in which inhibitor molecules may exist near interfaces and in the bulk aqueous phase, as indicated by the schematic phase diagram shown in Figure 9.

The long-term goal is to investigate and define the complete phase diagram shown in Figure 9. Once the relative stability of different phases as well as the transitions between the phases are determined, the dominant mechanisms by which inhibitor molecules adsorb, self-assemble on surfaces, and aggregate in the bulk phase will be understood. Clearly, getting to that level will take a few more years of concentrated effort; however, the most interesting learnings made on this journey so far are discussed below.

Fully atomistic simulations allow inclusion of chemical details in molecule definition and explicit representation of solvent molecules in the system. Specifically, the focus here was on studying model corrosion inhibitor molecules, such as imidazolinium-type and quaternary ammonium-type surfactants. Figure 10 shows the exact molecules that were studied so far: (a) two imidazolinium-type molecules: one with a 17 carbon long hydrophobic tail (Imid-17) and one with a 10 carbon long tail (Imid-10); and (b) two quaternary ammonium-type molecules: one with a 10 carbon long tail (Quat-10) and one with a 16 carbon long tail (Quat-16).[35] Simulations of these molecules in the bulk aqueous phase and near metal/water interfaces have provided interesting new insights, discussed below.

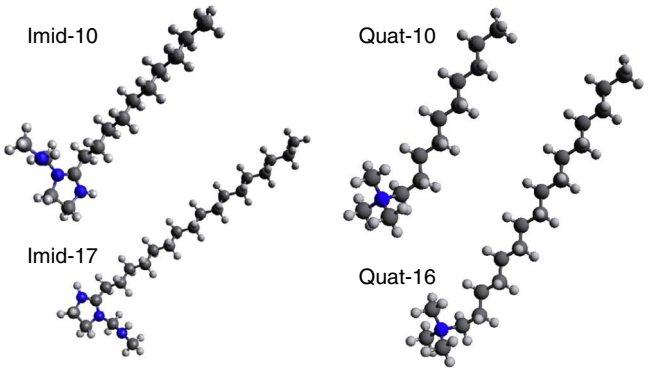


**FIGURE 10.** *The two imidazolinium-type (Imid-10 and Imid-17) and the two quaternary ammonium-type (Quat-10 and Quat-16) model corrosion inhibitor molecules used in the atomistic simulations. Blue beads represent the nitrogen atom, dark gray beads represent carbon atoms, and light gray beads represent hydrogen atoms.*

### *2.2.1 | Simulation Setup and System Details*

The imidazolinium-type and quaternary ammonium-type molecules are protonated at the polar group and therefore carry an overall charge of +1. In order to calculate partial charges on atoms of inhibitor molecules, B3LYP level DFT calculations were performed with 6-31G(d,p) orbital basis sets and implicit water using Gaussian 09† software.[36] From these DFT calculations, it can be observed that the +1 charge on the polar head group of imidazolinium-type molecules is delocalized among the two nitrogen atoms and the carbon atom in between them. The simulation system includes chloride ions to maintain the overall system charge neutrality. Water molecules are explicitly modeled using the single point charge enhanced (SPC/E) water model, which is a rigid, three-atom model. In the SPC/E model, there is a fixed partial charge of −0.8476e on the oxygen atom and +0.4238e on the hydrogen atoms, the H-O-H bond angle is 109.47°, and the O-H bond length is 1 Å (0.1 nm).[37] The metal surface is represented by six layers of a close-packed face-centered cubic (111) lattice plane of gold atoms with the lattice constant of 4.08 Å (0.408 nm). The gold surface is oriented parallel to the XY plane in the simulation box. Adsorption was studied on gold surface rather than on iron because the force field parameters for gold are available in the interface force field. While this is a drawback if one seeks to understand the adsorption of corrosion inhibitor molecules on steel, the authors believe that the general features of the adsorption behavior captured on a gold surface will be similar to that on an iron surface. This is because just like iron, gold has strong affinity for water as well as surfactants and is highly polarizable. Furthermore, previous researchers have studied adsorption of corrosion inhibitor molecules on gold surfaces via QCM experiments and have reported similar adsorption behavior.[38]

The simulation box is periodic in the X and Y directions, in the same way as was done above for CG simulations. On the face opposite to the gold surface, a noninteracting reflecting surface is placed to keep the simulation system volume constant. The dimensions of the simulation box is 52 Å by 54 Å by 190 Å (5.2 nm by 5.4 nm by 19 nm). The simulation box is significantly larger in the Z dimension to ensure that the liquid column placed over the gold surface is representative of the bulk aqueous phase. The interactions of gold atoms with other species are modeled using the interface force field.[39-40] The interface force field is parameterized in the functional form of LJ potential. The parameterization is done to reproduce the interfacial tension and bulk density of metals. The interactions of corrosion inhibitor molecules with other species is modeled using the general amber force field (GAFF), which is a widely used force field for surfactants and organic molecules.[41] In the GAFF force field, the nonbonded interactions between atoms is represented by LJ and Coulombic potentials. The bond and angle potentials are represented by harmonic functions. Along with these, there is potential energy associated with dihedral angles in molecular segments. The force field parameters in GAFF are determined by fitting many experimentally determined properties, such as densities, enthalpies of vaporization, bond vibration frequencies, etc.[41-42] The interaction parameters of chloride ions are from the Joung-Cheatham model,[43] which is a widely used force field for alkali and halide ions in explicit water. In the Joung-Cheatham model, the interaction potentials of monovalent ions are represented by LJ and Coulombic potentials. The potential parameters are fitted to hydration free energies, lattice energies, and lattice constants.

Total number of water molecules in the simulation system was 15,000. All simulations are performed at a temperature of T = 300 K. The simulations are performed in the canonical ensemble, that is, by keeping the temperature, volume, and total number of molecules in the system fixed. In order to maintain the pressure in the simulation system at saturation pressure, a vapor space of width ~5 Å (~0.5 nm) is created at the top of the simulation box.[35] This methodology is used because a constant temperature and pressure MD simulation requires adjustment of the simulation box size, which is not possible in this system because of the presence of a lattice of gold atoms.

For comparison purposes, atomistic MD simulations of corrosion inhibitor molecules in the bulk aqueous phase were also performed, that is, in the absence of a solid metal surface. In these simulations, the simulation box was periodic in all three directions. These atomistic MD simulations were also performed at the temperature of T = 300 K. The size of the simulation box is 50 Å × 50 Å × 50 Å (5 nm × 5 nm × 5 nm). The number of water molecules in the simulation box is ~3,500.

All MD simulations were performed using LAMMPS†.[22] For bulk simulations, constant temperature and pressure MD simulations were performed (P = 1 bar [100 kPa]). The atomistic MD simulations were performed in parallel on 28 processors. For the micelle formation studies (discussed below), 31 ns to 46 ns long MD simulations were performed. Approximately 3 ns of atomistic MD simulation takes 1 d on 28 processors. For free energy calculations using umbrella sampling (discussed below), 64 different umbrella sampling windows of 6 ns to 9 ns each were generated for each free energy calculation.

### *2.2.2 | Results*

#### *2.2.2.1 | Micelle Formation in the Bulk Solution and Their Characteristics Depend on the Type of Inhibitor Molecule*

At concentrations above the critical micelle concentration (CMC), inhibitor molecules are expected to aggregate as micelles. It was found that both groups of molecules Imid-10/Imid-17 and Quat-10/Quat-16 molecules aggregate into micelles with a roughly spherical shape. Figure 11 shows snapshots of the micelles formed by different compounds with different numbers of molecules. In these micelles, the hydrophobic alkyl tails of the molecules form the core, while the polar head groups remain on the periphery, facing the water molecules.

From Figure 11, the Imid micelles appear to be more densely packed than the Quat micelles. Indeed, the calculated

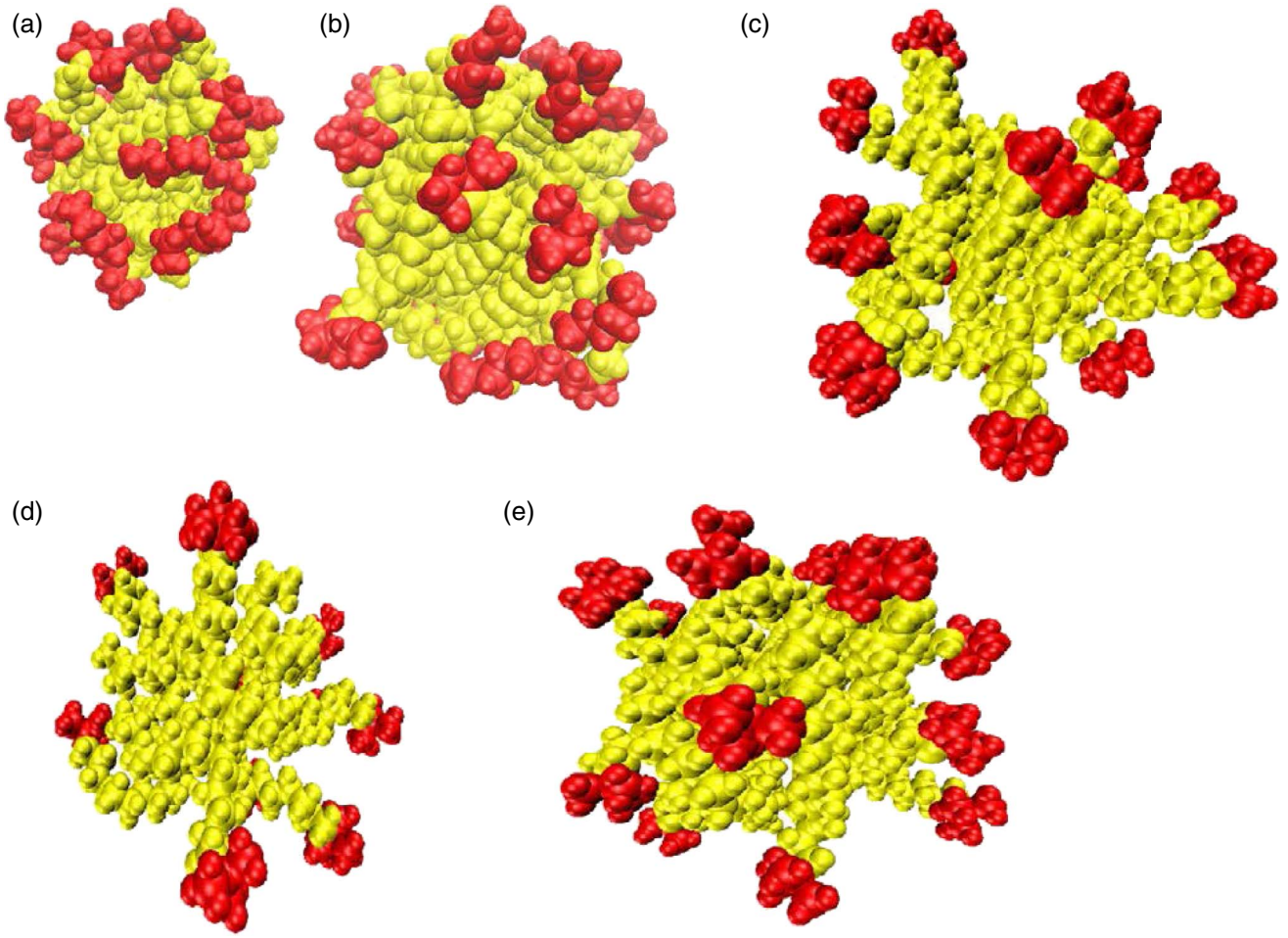


**FIGURE 11.** *Snapshots of (a) an Imid-10 micelle consisting of 18 molecules, (b) an Imid-17 micelle consisting of 19 molecules, (c) a Quat-10 micelle consisting of 18 molecules, and (d) and (e) Quat-16 micelles with consisting of 10 and 19 molecules, respectively. Yellow segments represent the alkyl tails, and red segments represent the polar head group.*

number density of Imid-10 micelle consisting of 18 molecules is 0.28 heavy atoms/Å$^3$, whereas that of Quat-10 micelle with 18 molecules is 0.26 heavy atoms/Å$^3$. For Imid-17 micelle with 19 molecules, the number density is 0.35 heavy atoms/Å$^3$, while that of Quat-16 with 19 molecules is 0.30 heavy atoms/Å$^3$. Hence, in general, Imid micelles have a higher number density as compared to the Quat micelles. Furthermore, in the Quat micelles, the polar head group seems to protrude out of the micelle, which is not seen for Imid micelles. This difference in micellar structure could be because in Quat molecules, the charge on the polar head group is localized on the nitrogen atom, while in Imid molecules, the charge is delocalized partially on the imidazoline ring, which reduces Coulombic interactions in case of Imid molecules.

The asphericity of Imid-10 and Imid-17 micelles comprised of different number of molecules, $N_{micelles}$, is plotted in Figure 12(a). It is observed that except for small sized-micelles ($N_{micelles} \leq 5$), the asphericity is small, indicating that the micelles are pretty much spherical in shape.

Diffusion coefficient of micelles of different sizes calculated from the simulations are shown in Figure 12(b). In these simulations, the concentration of Imid-10/Imid-17 molecules in the system was kept the same for all micelles, equal to 0.09 M. Diffusion coefficient was calculated by using Einstein's relation, which states that <MSD> = 6Dt, where <MSD> stands for average mean square displacement, D is the diffusion coefficient, and t is the time. As expected, D decreases as the micelles become bigger. Imid-10 micelles have larger D as compared to Imid-17 micelles, owing to their smaller size.

### *2.2.2.2 | Corrosion Inhibitor Molecules Form Micelles near the Metal/Water Interface*

As a first step towards understanding the behavior of corrosion inhibitor molecules and their adsorption on metal surfaces, a gold surface was introduced at the bottom of the simulation box as indicated in Figure 13. After reaching equilibrium, the following observations could be made: (a) most inhibitor molecules aggregated in the aqueous phase as micelles and did not adsorb on the metal surface; and (b) few inhibitor molecules (4 to 5 out of 64) adsorbed on the metal surface with the alkyl tails lying flat on the metal surface. The underlying reasons for these observations will be discussed below.

These results suggest that corrosion inhibitors aggregated in micelles have a weak tendency to adsorb on to a metal surface. On the other hand, unaggregated corrosion inhibitor molecules have a strong tendency to adsorb. To further understand the adsorption behavior, the free energy of

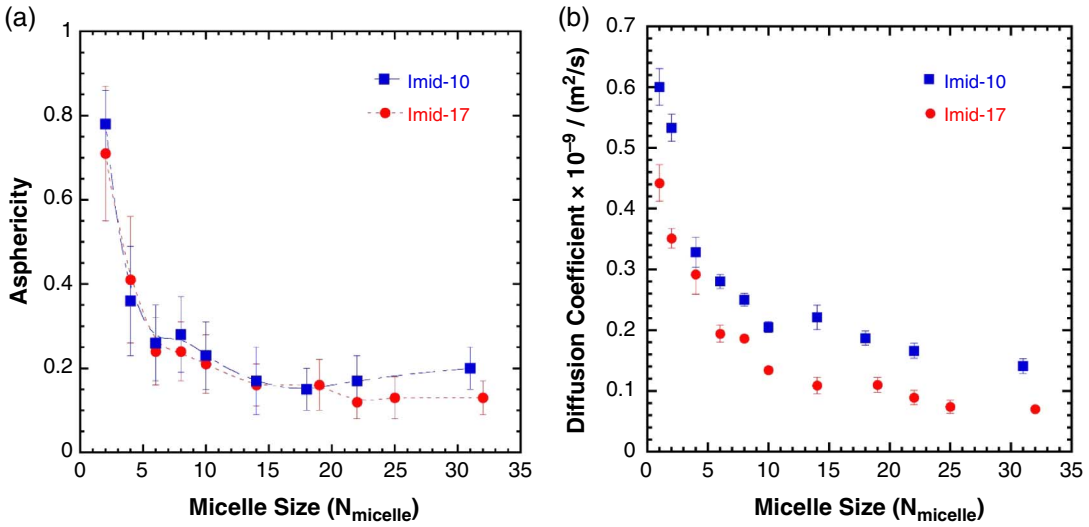


**FIGURE 12.** *(a) Asphericity, and (b) diffusion coefficient of Imid-10 and Imid-17 micelles comprised of different number of molecules, $N_{micelle}$.*

adsorption of corrosion inhibitor molecules in infinite dilution and in the micellar state were calculated.

### *2.2.2.3 | Unaggregated Corrosion Inhibitor Molecules Show a Strong Tendency to Adsorb onto the Metal Surface*

For both Imid-10 and Imid-17 molecules, the free energy of adsorption in infinite dilution was calculated using a simulation methodology called "umbrella sampling."[44] Before discussing the results, a brief introduction to free energy calculations and the umbrella sampling methodology might be helpful. Recall that for a closed system, that is, for a system with fixed number of particles N, volume V, and temperature T, thermodynamic equilibrium is reached when the Helmholtz free energy F is minimized. Therefore, in a canonical ensemble MD simulation (using a system with constant number of molecules in a constant volume at constant temperature), the equilibrium state will be a local minimum of the free energy landscape. Suppose one is interested in studying the transition from one thermodynamic state A to another state B. This transition can be followed by calculating the value of some thermodynamic variable, termed as reaction coordinate, which is a measure of the path traversed from A to B. For example, adsorption transition of a molecule from the bulk aqueous phase onto the metal surface can be followed by the reaction coordinate defined as the distance between the center of mass of the molecule and the metal surface, ξ. If, for each value of the reaction coordinate ξ, one calculates F(ξ), then one has determined the free energy profile of the system transitioning from state A to state B.

However, there are certain problems associated with directly calculating F(ξ). If the states A and B are both local minimum of the free energy landscape, then a straightforward MD simulation will either equilibrate to the state A or to the state B, and will only sparsely sample state points in between A and B. Hence, to generate F(ξ) for all ξ, the umbrella sampling methodology comes in handy. In umbrella sampling, a harmonic bias potential of the form, $U_{bias} = k(\xi - \xi_o)^2$, where ξ is the instantaneous value of the reaction coordinate and $\xi_o$ is the set-value, is applied. The bias potential ensures that the simulation system samples state points close to $\xi_o$. By systematically changing the value of $\xi_o$ in a series of MD simulations, one can sample all values of ξ between the states A and B. From the biased sampling so obtained from umbrella sampling simulations, one can determine unbiased free energies, F(ξ), by invoking laws of statistical mechanics. Specifically, a procedure known as weighted histogram analysis method (WHAM) has been used for un-biasing these simulations. Discussion of WHAM equations is beyond the scope of this paper, but an interested reader can refer to the cited publication.[45]

Now getting back to the results: Figure 14 shows free energy profiles of adsorption of Imid-10 and Imid-17 molecules on to the metal surface at infinite dilution.[35] Clearly, both inhibitor molecules demonstrate a strong tendency to adsorb with no free energy barrier to adsorption. The adsorption free energy is found to be ~30 $k_BT$. Furthermore, the affinity to adsorb for both the molecules is found to be similar. The Imid-17 molecule has a larger enthalpy of adsorption on the metal surface, owing to its longer alkyl tail; however, its adsorption is also accompanied by a larger entropic loss.[35] Hence, there is an enthalpy-entropy compensation between these two molecules, which results in similar free energy of adsorption.

The free energy profiles are not smooth. This is because the orientational space of the molecules was not exhaustively sampled. Ideally, one can do so by applying another harmonic bias potential in the orientational space. However, such a calculation will require at least an order of magnitude more simulations. In Figure 14 (inset), a snapshot of an adsorbed configuration of Imid-17 molecule is shown. The molecule adsorbs with the alkyl tail lying flat on the metal surface because in this configuration the alkyl tail as well as the polar head group of the molecule are able to interact favorably with the metal surface.

### *2.2.2.4 | Micelles of Corrosion Inhibitor Molecules Have a Weak Tendency to Adsorb onto the Metal Surface*

To study the adsorption behavior of inhibitor micelles formed in the bulk, adsorption free energy profiles of Imid-10 and Imid-17 micelles comprised of 18 and 19 molecules, respectively, were calculated using umbrella sampling. For this calculation, the reaction coordinate, ξ, is chosen as the

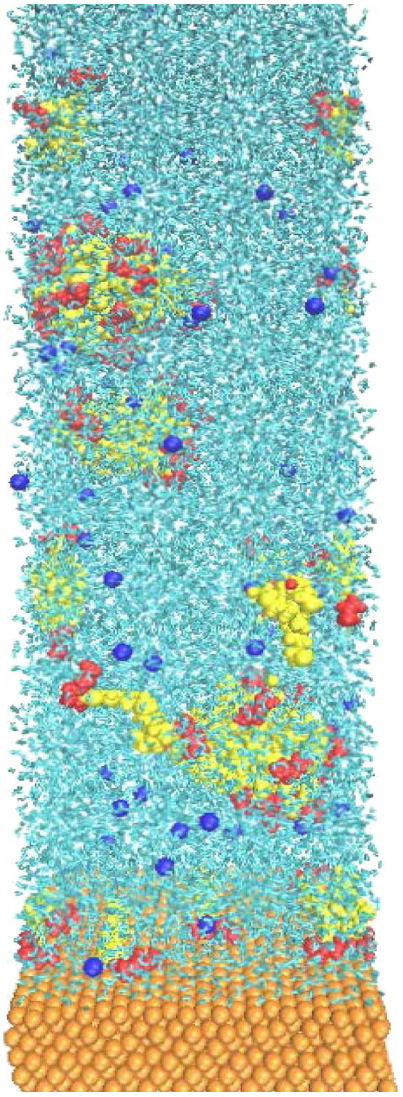

**FIGURE 13.** *A snapshot of the simulation system with 64 Imid-17 molecules in water near a gold lattice, yellow atoms are parts of alkyl tails, red atoms are parts of polar head groups, golden color atoms represent gold atoms, blue represents chloride ions, and cyan represent water molecules. Adapted with permission from Kurapati and Sharma.*[35]

distance between the center of mass of the micelle and the metal surface. Figure 15 shows the free energy profiles.[35] It is observed that the inhibitor micelles experience a repulsion from the metal surface at distances as large as 50 Å to 60 Å (5 nm to 6 nm). The repulsion is long-ranged considering that the radius of these micelles is ~15 Å (~1.5 nm). This long-ranged repulsion is observed because the micelles are surrounded by a large corona of counter-ions as well as their solvation shells.[35] This corona of the micelle is disturbed as the micelle approaches the metal surface which gives rise to the observed repulsion.

Furthermore, the free energy profiles have a maximum at a ξ of 21 Å (2.1 nm) followed by a local minimum. This maximum in the free energy profile corresponds to the removal of adsorbed layers of water on the metal surface.[35] At the location of local minimum (~15 Å [1.5 nm]), the micelles are in contact with the metal surface.

Figure 16 shows a snapshot of the Imid-17 micelle in contact with the metal. In the simulations, micelles breaking apart upon adsorption were not observed. It is interesting to compare these profiles with the ones obtained for the infinite dilution case (Figure 14). While the unaggregated molecules show a strong tendency to adsorb on to the metal surface, the micelles experience a long-range repulsion from the surface. These results explain why in the straightforward MD simulations, it was found that most inhibitor molecules in the micellar form do not adsorb, whereas some unaggregated molecules adsorb on the surface.

### *2.2.2.5 | Adsorbed Layer of Corrosion Inhibitors*

In the CG molecular simulations, it was shown that the nature of the adsorbed layer of inhibitor molecules depends on the ratio $\frac{E_{standing}}{E_{lying}}$ given by Equation (9). For the fully atomistic model of corrosion inhibitors, this ratio is calculated using interaction parameters of the force field ($\varepsilon_s$ = 7.55 Kcal/mol, $\varepsilon_t$ = 2.21 Kcal/mol) and molecular properties ($A_c$ = 0.14 $nm^2$, l = 1.5 nm [Quat-10] / 2.3 nm [Quat-16], n = 10 [Quat-10] / 16 [Quat-16], f = 0.57). This ratio is estimated to be roughly 0.45, which indicates that the adsorbed layer should comprise of inhibitor molecules lying flat on the surface. In order to study the nature of the adsorbed layer, an initial configuration was created wherein Quat-10/Quat-16 inhibitor molecules are arranged in a planar arrangement over a gold surface (Figure 17[a]). Starting from this initial configuration, isothermal-isobaric ensemble MD simulations were performed at temperature T = 300 K.

After an extremely long simulation of 320 ns, the adsorbed layer of inhibitor molecules was observed undergoing a significant rearrangement wherein the molecules eventually end up adsorbing parallel to the surface (Figure 17[b]). Because of the space constraint, the remaining molecules desorb and aggregate in micellar form in the bulk phase. While these results align well with the theoretical model of Equation (9) and CG simulations, they are in contrast with the typical interpretations stemming from experimental studies, where it is stated that corrosion inhibitor molecules adsorb with their polar groups toward the metal surface and the hydrophobic tails pointing toward the solution. A source of discrepancy could be that the strength of interaction between the polar-head group and the metal surface is stronger than what was in this model (indicating possibly a much stronger physical or chemical interaction). This aspect will be explored further in future work.

To summarize, through atomistic MD simulations, it is revealed that unaggregated corrosion inhibitor molecules exhibit strong affinity toward adsorption. On the other hand, micelles of corrosion inhibitor molecules have a weaker tendency to adsorb and are metastable in the adsorbed state. A decrease in adsorption with the aggregation of inhibitor molecules in the bulk phase is also observed in the CG simulations (Figure 3), but this effect is more pronounced in atomistic simulations wherein water and counter-ions are explicitly included in the system. At infinite dilution, the inhibitor molecules adsorb with their alkyl tails parallel to the metal surface because of affinity of the tail for the metal. In the adsorbed layer as well, the inhibitor molecules are found to adsorb with their alkyl tails parallel to the metal surface. These results are in contrast with typical interpretations which have corrosion inhibitor molecules arranging themselves in SAM with polar group towards the metal surface and alkyl tail towards water.

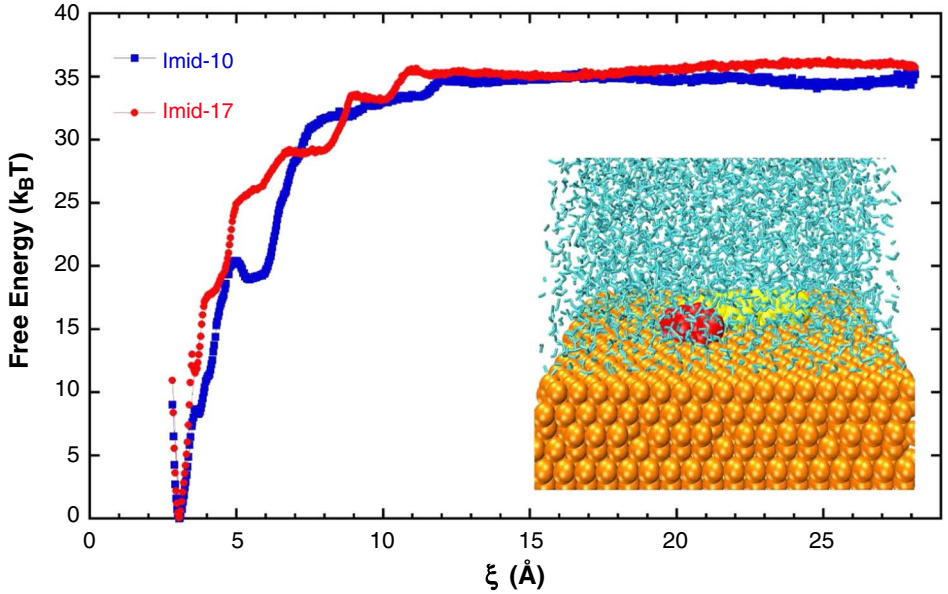


**FIGURE 14.** *Free energy of adsorption profiles for Imid-10 and Imid-17 molecules on a gold lattice at infinite dilution; inset: equilibrium adsorbed configuration of the Imid-17 molecule. Adapted with permission from Kurapati and Sharma.*[35]

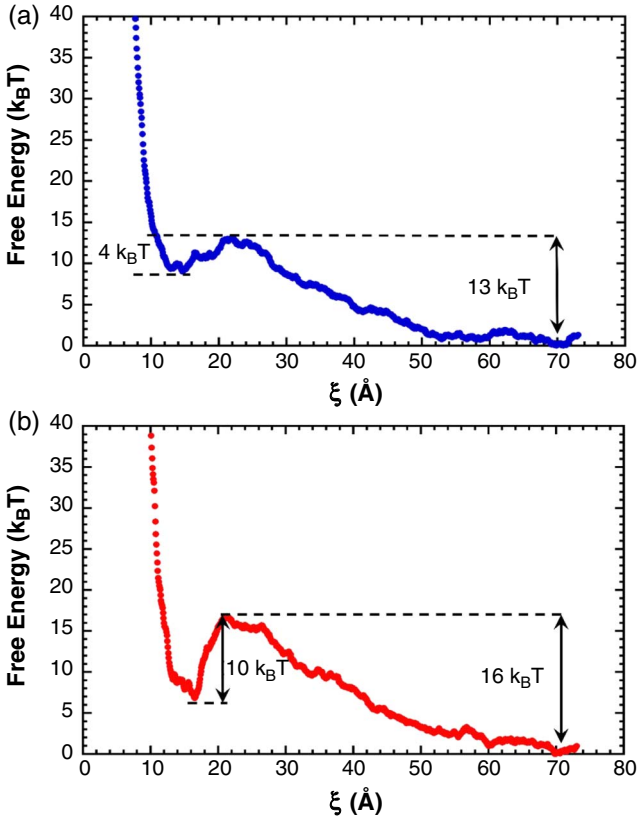


**FIGURE 15.** *Free energy profiles of adsorption of (a) Imid-10 micelle, and (b) Imid-17 micelle comprised of 18 and 19 molecules, respectively. Adapted with permission from Kurapati and Sharma.*[35]

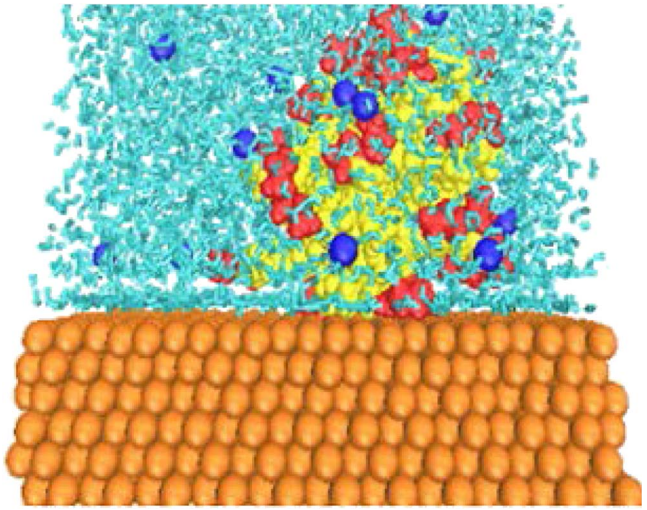

**FIGURE 16.** *A snapshot of an Imid-17 micelle adsorbed on the metal surface. Adapted with permission from Kurapati and Sharma.*[35]

## SUMMARY, CAVEATS, AND FUTURE WORK

Classical molecular simulations complement experiments in deciphering the behavior of physical systems by providing a window to observe the nanoscale. In this paper, recent efforts in using molecular simulations to understand adsorption, aggregation, and self-assembly of corrosion inhibitor molecules on metal surfaces are discussed. New insights have emerged from these simulations, which in some cases, challenge the long-standing presumptions, and in other cases, validate them. Major findings from these coarse-grained simulations are that (a) hydrophobic interactions play an important role in the adsorption and self-assembly processes, (b) molecular geometry has a significant effect on the morphology of the adsorbed layer, and (c) the relative strength of polar head-metal and alkyl tail-metal interactions are important determinants of adsorbed conformations. The atomistic simulations reveal that the adsorption behavior of inhibitor molecules is strongly dependent on their aggregation state. While unaggregated molecules have a strong tendency to adsorb on to the metal surface, micelles experience

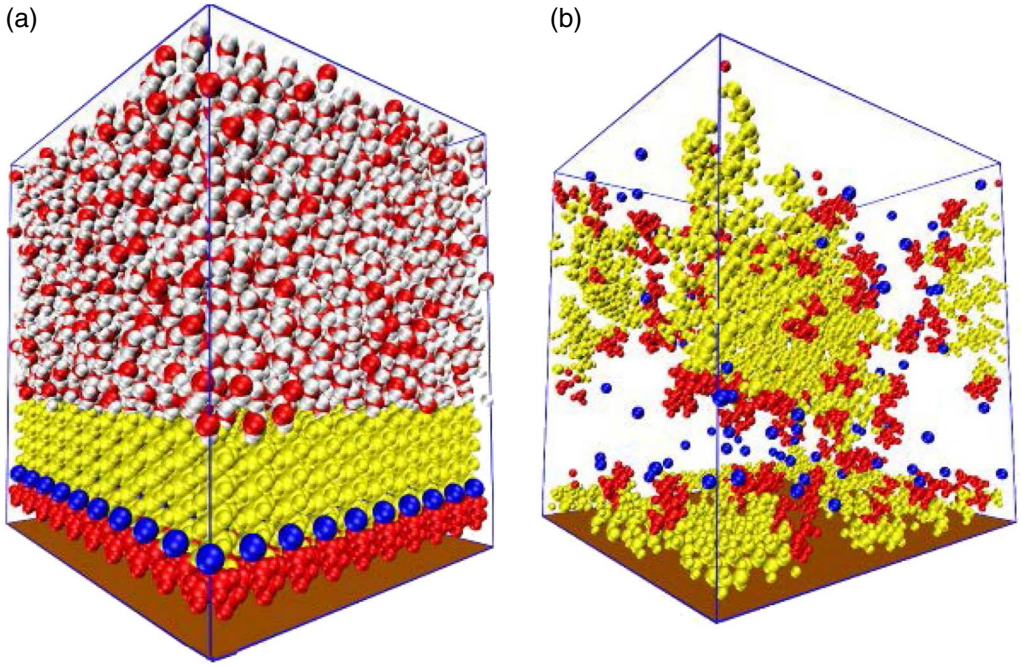


**FIGURE 17.** *(a) A snapshot of initial configuration of simulation system with an adsorbed layer of Quat-10 molecules on the gold surface. Yellow represents the alkyl tails, red represents the polar head group, and blue represents chloride. Water molecules are represented by red (oxygen) and white (hydrogen). (b) A snapshot of the simulation system after 320 ns of MD simulation (water molecules not shown for clarity).*

a long-range repulsion from the surface. This result suggests that efficient corrosion inhibition will be observed at corrosion inhibitor concentrations below the critical micelle concentration (CMC) because unaggregated molecules readily adsorb. On the other hand, above the CMC, the inhibitor molecules form micelles which show a weak tendency to adsorb.

These are useful results which will help researchers in corrosion inhibition to develop better strategies to design and deploy corrosion inhibitors for field applications. That said, it will be appropriate to comment that this has so far only "scratched the surface" and a lot more information can be gained from molecular simulations of these systems. There is a need to systematically explore how the adsorption and aggregation behavior changes as the chemistry of the molecules is changed, and how the physical properties of the metal/water interfaces are affected as a result. The results of these simulations will be on a stronger footing once their predictions are validated via synergistic experiments. Furthermore, the sensitivity of the results on the models used in these simulations needs to be carefully examined. In the CG simulations, the effect of water is incorporated through an effective hydrophobic attraction between alkyl tails and Langevin dynamics, which mimics random collisions between solute and solvent molecules. However, in the absence of explicitly represented water molecules, many differences in the simulation results may occur. The atomistic simulations show that near metal surfaces, the water molecules arrange in two layers. Furthermore, in the atomistic simulations it was observed that the interactions between the solvation shell of inhibitor micelles and the adsorbed layers of water result in a long-range repulsion between the micelles and the surface. These effects will not be observed in the case of implicitly-included water.

Finally, it is important to mention some caveats of molecular simulations. Certain assumptions and simplifications are made in designing the simulation systems, which can be a source of errors in the results. First, the force fields used in molecular simulations are developed by fitting simulations results to some thermodynamic properties determined from experiments. Hence, the designed force fields may be good at reproducing some thermodynamic properties but not others. These force fields are assumed to be transferable from one system to another, which may not always be the case. Furthermore, polarizability of different species is often ignored in molecular simulations. Some polarizable force fields have been developed, but their performance are not observed to be overall better than that of nonpolarizable force fields, and hence they have not become popular. Classical molecular simulations cannot capture chemical reactions, such as bond forming or breaking, which may occur in some systems. Because of the computational complexity of molecular simulations, the system sizes are of the order of 10 nm to 100 nm. As a result, the concentration of solutes in the simulations is often taken to be higher than in experiments.

## ACKNOWLEDGMENTS

Acknowledgment is made to the donors of the American Chemical Society Petroleum Research Fund (ACS PRF No. 56892-DNI6) for support of this research. This work is partially supported by the NSF CBET Grant No. 1705817. The authors thank researchers at the Institute for Corrosion and Multiphase Technology (ICMT) for useful discussions. Computational resources for this work were provided by the Ohio Supercomputer Center.

### References

1. M. Finšgar, J. Jackson, *Corros. Sci.* 86 (2014): p. 17-41.
2. A.J. McMahon, *Colloid Surf.* 59 (1991): p. 187-208.
3. Y.-J. Tan, S. Bailey, B. Kinsella, *Corros. Sci.* 38, 9 (1996): p. 1545-1561.

4. X. Liu, S. Chen, F. Tian, H. Ma, L. Shen, H. Zhai, *Surf. Interface Anal.* 39, 4 (2007): p. 317-323.
5. J. Cruz, R. Martínez, J. Genesca, E. García-Ochoa, *J. Electroanal. Chem.* 566, 1 (2004): p. 111-121.
6. Y. Xiong, B. Brown, B. Kinsella, S. Nešić, A. Pailleret, *Corrosion* 70, 3 (2014): p. 247-260.
7. I. Jevremović, M. Singer, S. Nešić, V. Mišković-Stanković, *Corros. Sci.* 77 (2013): p. 265-272.
8. A. Edwards, C. Osborne, S. Webster, D. Klenerman, M. Joseph, P. Ostovar, M. Doyle, *Corros. Sci.* 36, 2 (1994): p. 315-325.
9. H.O. Curkovic, E. Stupnisek-Lisac, H. Takenouti, *Corros. Sci.* 51, 10 (2009): p. 2342-2348.
10. Z.D. Schultz, M.E. Biggin, J.O. White, A.A. Gewirth, *Anal. Chem.* 76, 3 (2004): p. 604-609.
11. A. Kokalj, *Corros. Sci.* 68 (2013): p. 195-203.
12. G. Gece, *Corros. Sci.* 50, 11 (2008): p. 2981-2992.
13. N. Kovačević, I. Milošev, A. Kokalj, *Corros. Sci.* 124 (2017): p. 25-34.
14. S. Xia, M. Qiu, L. Yu, F. Liu, H. Zhao, *Corros. Sci.* 50, 7 (2008): p. 2021-2029.
15. Y. Tang, L. Yao, C. Kong, W. Yang, Y. Chen, *Corros. Sci.* 53, 5 (2011): p. 2046-2049.
16. M.P. Allen, D.J. Tildesley, *Computer Simulation of Liquids* (Oxford, United Kingdom: Oxford University Press, 1989).
17. Y. Duda, R. Govea-Rueda, M. Galicia, H.I. Beltrán, L.S. Zamudio-Rivera, *J. Phys. Chem. B* 109, 47 (2005): p. 22674-22684.
18. R. Wu, M. Deng, B. Kong, X. Yang, *J. Phys. Chem. B* 113, 45 (2009): p. 15010-15016.
19. X. Ko, S. Sharma, *J. Phys. Chem. B* 121, 45 (2017): p. 10364-10370.
20. J.D. Weeks, D. Chandler, H.C. Andersen, *J. Chem. Phys.* 54, 12 (1971): p. 5237-5247.
21. N. Choudhury, B.M. Pettitt, *J. Am. Chem. Soc.* 127, 10 (2005): p. 3556-3567.
22. S. Plimpton, *J. Comput. Phys.* 117, 1 (1995): p. 1-19.
23. P. Somasundaran, D.W. Fuerstenau, *J. Phys. Chem.* 70, 1 (1966): p. 90-96.
24. A. Fan, P. Somasundaran, N.J. Turro, *Langmuir* 13, 3 (1997): p. 506-510.
25. R. Atkin, *J. Colloid Interf. Sci.* 266, 2 (2003): p. 236-244.
26. T.P. Goloub, L.K. Koopal, *Langmuir* 13, 4 (1997): p. 673-681.
27. V. Padmanabhan, S.K. Kumar, A. Yethiraj, *J. Chem. Phys.* 128, 12 (2008): p. 124908.
28. H. Arkın, W. Janke, *J. Chem. Phys.* 138, 5 (2013): p. 054904.
29. S. Abbott, *Surfactant Science: Principles and Practice* (Steven Abbott, 2015), http://www.stevenabbott.co.uk/practical-surfactants/the-book.php (Sept. 9, 2017).
30. S. Manne, J.P. Cleveland, H.E. Gaub, G.D. Stucky, P.K. Hansma, *Langmuir* 10, 12 (1994): p. 4409-4413.
31. S. Manne, T.E. Schäffer, Q. Huo, P.K. Hansma, D.E. Morse, G.D. Stucky, I.A. Aksay, *Langmuir* 13, 24 (1997): p. 6382-6387.
32. R. Zhang, P. Somasundaran, *Adv. Colloid Interface Sci.* 123 (2006): p. 213-229.
33. R. Atkin, V.S.J. Craig, E.J. Wanless, S. Biggs, *Adv. Colloid Interface Sci.* 103, 3 (2003): p. 219-304.
34. D.K. Schwartz, *Annu. Rev. Phys. Chem.* 52, 1 (2001): p. 107-137.
35. Y. Kurapati, S. Sharma, *J. Phys. Chem. B* 122 (2018): p. 5933-5939.
36. M.J. Frisch, et al., *Gaussian 09* (Wallingford, CT: Gaussian, Inc., 2009).
37. H.J.C. Berendsen, J.R. Grigera, T.P. Straatsma, *J. Phys. Chem.* 91, 24 (1987): p. 6269-6271.
38. P. Kern, D. Landolt, *J. Electrochem. Soc.* 148, 6 (2001): p. B228-B235.
39. H. Heinz, T.-J. Lin, R. Kishore Mishra, F.S. Emami, *Langmuir* 29, 6 (2013): p. 1754-1765.
40. H. Heinz, R.A. Vaia, B.L. Farmer, R.R. Naik, *J. Phys. Chem. C* 112, 44 (2008): p. 17281-17290.
41. J. Wang, R.M. Wolf, J.W. Caldwell, P.A. Kollman, D.A. Case, *J. Comput. Chem.* 25, 9 (2004): p. 1157-1174.
42. W.D. Cornell, P. Cieplak, C.I. Bayly, I.R. Gould, K.M. Merz, D.M. Ferguson, D.C. Spellmeyer, T. Fox, J.W. Caldwell, P.A. Kollman, *J. Am. Chem. Soc.* 117, 19 (1995): p. 5179-5197.
43. I.S. Joung, T.E. Cheatham III, *J. Phys. Chem. B* 112, 30 (2008): p. 9020-9041.
44. G.M. Torrie, J.P. Valleau, *J. Comput. Phys.* 23, 2 (1977): p. 187-199.
45. S. Kumar, J.M. Rosenberg, D. Bouzida, R.H. Swendsen, P.A. Kollman, *J. Comput. Chem.* 13, 8 (1992): p. 1011-1021.